Detailed Structural and Theoretical Studies of the Bonding in Edge-Bridged Halide and Oxyhalide Octahedral Niobium and Tantalum Clusters

François Ogliaro, Stéphane Cordier, Jean-François Halet,* Christiane Perrin,* Jean-Yves Saillard,* and Marcel Sergent

Laboratoire de Chimie du Solide et Inorganique Moléculaire, UMR CNRS 6511, Université de Rennes 1, Avenue du Général Leclerc, 35042 Rennes Cedex, France

Received March 24, 1998

New $A_xREM_6X_{18}$ (A = monovalent cation; RE = rare-earth metal; M = Nb, Ta; X = Cl, Br; x = 0, 1, 2), $A_2REM_6X_{18-y}O_y$ (y = 1, 3) and $REM_6X_{13}O_3$ containing edge-bridged octahedral $(M_6X^i_{12})X^a_6$ units are obtained in sealed silica tubes at 700 °C. The structures of $CsErTa_6Cl_{18}$ and $Cs_2UTa_6Cl_{15}O_3$ were established by single-crystal X-ray diffraction. They both crystallize in the $P\bar{3}1c$ space group (a = 9.239(2) Å, c = 17.233(7) Å and a = 9.1824(5) Å, c = 17.146 (2) Å, respectively). Features which act to stabilize this type of cluster compound are analyzed. Density functional theory (DFT) calculations were carried out in order to learn more about the relationships that exist between their structural arrangement and the number of electrons available for metal−metal bonding in M_6 clusters. In particular, DFT results show that valence electron counts (VEC) from 14 to 16 are possible for the same octahedral $M_6X^i_{12}X^a_6$ arrangement because of a nonbonding (M−M bonding and M−X^i antibonding) MO lying in the middle of a large energy gap separating a bonding set of MOs from an antibonding set of MOs. Replacing one X ligand by a less-hindered oxygen ligand does not modify much the electronic structure of these species. Stable $M_6X_{17}O$ units with different electron counts are theoretically possible. In contrast, a larger number of oxygen ligands perturbs the electronic structure, and 14-electron species are likely to be trapped, as experimentally observed in the case of compounds containing $M_6X_{15}O_3$ units.

Introduction

Since their first structural characterization in solution in the 1950s in Pauling's laboratory,[1] edge-bridged octahedral cluster compounds of general formula $[(M_6X^i_{12})L^a_6]^{n-}$ (M = Nb, Ta; X^i = two-bonded inner halide ligand; L^a = two-electron donor apical ligand (H_2O, OH^-, Cl^-, Br^-...)), **1** (Chart 1), dominates niobium and tantalum halide cluster chemistry.[2,3] Nevertheless, despite the numerous experimental and theoretical studies devoted to these compounds,[2−5] no systematic detailed analysis has been done so far concerning the features which act to their stabilization. Recently in our laboratory, we have investigated solid-state materials with the general formula $A_xREM_6X_{18}$ (A = monovalent cation; RE = rare-earth metal in general; M = Nb, Ta; X = Cl, Br; x = 0, 1, 2), $A_2REM_6X_{18-y}O_y$ (y = 1, 3) and $REM_6X_{13}O_3$ containing this kind of edge-bridged octahedral $(M_6X^i_{12})X^a_6$ unit.[6] Changing the nature of the different constituting elements has led to a set of new isostructural compounds, allowing a rigorous structural analysis of these units upon the number of electrons available for metal−metal bonding (the so-called cluster valence electron count, VEC) and the electronic and size effects of the metal atoms and the ligands. For instance, the partial replacement of halogen ligands by oxygen ligands leads for the first time to the preparation of oxyhalide Nb_6 and Ta_6 clusters, providing information on the structural distortion of the cluster core upon halide substitution.[7−9]

Chart 1

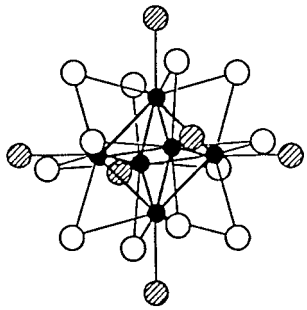

1

The aim of this paper is to understand the stability of such octahedral cluster compounds. We use here all our recent experimental results, including the new $CsErTa_6Cl_{18}$ and $Cs_2UTa_6Cl_{15}O_3$ compounds structurally characterized by single-crystal X-ray diffraction, to analyze the features which act to stabilize this type of architecture. These experimental results are accompanied with density functional theory (DFT) calcula-

(1) Vaughan, P. A.; Sturtivant, J. H.; Pauling, L. *J. Am. Chem. Soc.* **1950**, *72*, 5477.
(2) Schäfer, H.; von Schnering, H. G. *Angew. Chem.* **1964**, *76*, 833.
(3) (a) Simon, A. In *Handbook on the Physics and Chemistry of Rare Earths*; Gschneider, K. A., Jr.; Eyring, L., Eds; Elsevier Science Publishers B.V.: New York, 1991; Vol. 15, p 195. (b) Simon, A. In *Clusters and Colloids*: *From Theory to Applications*; Schmid, G., Ed.; VCH: Weinheim, 1994 and references therein.
(4) Cotton, F. A.; Haas, R. E. *Inorg. Chem.* **1964**, *3*, 10.
(5) For some leading reviews, see: (a) Hughbanks, T. *Prog. Solid State Chem.* **1989**, *19*, 329. (b) Lin, Z.; Williams, I. D. *Polyhedron* **1996**, *15*, 3277. (c) Lin, Z., Fan, M.-F. *Struct. Bonding* **1997**, *87*, 35 and references therein.
(6) Perrin, C.; Cordier, S.; Ihmaïne, S.; Sergent, M. *J. Alloys Compd.* **1995**, *229*, 123 and references therein.
(7) Cordier, S.; Perrin, C.; Sergent, M. *Eur. J. Solid State Inorg. Chem.* **1994**, *31*, 1049.
(8) Cordier, S.; Perrin, C.; Sergent, M. *J. Solid State Chem.* **1995**, *120*, 43.
(9) Cordier, S.; Perrin, C.; Sergent, M. *Mater. Res. Bull.* **1996**, *31*, 683.

10.1021/ic980328h CCC: $15.00
Published on Web 10/31/1998

Table 1. Crystallographic Data for $CsErTa_6Cl_{18}$

space group: $P\bar{3}1c-D_{3d}^2$, No. 163, origin at $\bar{3}$	
$a = 9.239(2)$ Å	$\lambda = 0.710\ 73$ Å
$c = 17.233(7)$ Å	$T = 293$ K
$V = 1274.0(5)$ Å^3	$Z = 2$
fw = 2024.01	$\rho = 5.27$ g cm^{-3}
2321 measd reflcns	1658 indep reflcns ($R_{int} = 0.022$)
1482 reflcns used in the refinement with $I > 3\sigma(I)$	
DIFABS[12] ($T_{min} = 0.611$, $T_{max} = 1.082$)	$\mu = 319.7$ cm^{-1}
$R^a = 0.034$	$R_w{}^b = 0.048$
GOF$^c = 1.55$	

$^a R = \sum||F_o| - |F_c||/\sum|F_o|$. $^b R_w = [\sum w(|F_o| - |F_c|)^2/\sum|F_o|^2]^{1/2}$; $w = 4F_o^2/[\sigma(F_o^2)^2 + (0.04F_o^2)^2]$. The goodness of fit is defined as $[w(|F_o| - |F_c|)^2/(n_o - n_v)]^{1/2}$, where n_o and n_v denote the numbers of data and variables, respectively.

Table 2. Crystallographic Data for $Cs_2UTa_6Cl_{15}O_3$

space group: $P\bar{3}1c-D_{3d}^2$, No. 163, origin at $\bar{3}$	
$a = 9.1824(5)$ Å	$\lambda = 0.710\ 73$ Å
$c = 17.146(2)$ Å	$T = 293$ K
$V = 1252.0(1)$ Å^3	$Z = 2$
fw = 2169.32	$\rho = 5.75$ g cm^{-3}
3008 measd reflcns	1589 indep reflcns ($R_{int} = 0.023$)
1281 reflcns used in the refinement with $I > 3\sigma(I)$	
ψ scans[12] ($T_{min} = 0.530$, $T_{max} = 0.999$)	$\mu = 363.9$ cm^{-1}
$R^a = 0.032$	$R_w{}^b = 0.034$
GOF$^c = 0.988$	

$^a R = \sum||F_o| - |F_c||/\sum|F_o|$. $^b R_w = [\sum w(|F_o| - |F_c|)^2/\sum|F_o|^2]^{1/2}$; $w = 4F_o^2/[\sigma(F_o^2)^2 + (0.04F_o^2)^2]$. The goodness of fit is defined as $[w(|F_o| - |F_c|)^2/(n_o - n_v)]^{1/2}$, where n_o and n_v denote the numbers of data and variables, respectively.

tions in order to learn more about the relationships that exist between their structural arrangement and the number of electrons available for metal−metal bonding in M_6 clusters.

Experimental Section

Preparation. Stoichiometric mixtures of CsCl (Prolabo, 99.5%), $ErCl_3$ (synthesized according to the procedure described ealier,[10] $TaCl_5$ (Alfa, 99.9%), Ta (Alfa, m3N,T2N6) for $CsErTa_6Cl_{18}$ and CsCl, UCl_4 (Prolabo, 99.5%), Ta_2O_5 (Ventron, 99.5%), $TaCl_5$, Ta for $Cs_2UTa_6Cl_{15}O_3$, were weighed and compacted under inert atmosphere and subsequently heated at 700 °C for 24 h in silica tubes sealed under dynamic vacuum. Single crystals of the two compounds, suitable for structural determination, were directly obtained during a synthesis of 1 week, starting from a nonpelletized mixture. A similar technique was used to prepare all the Nb_6 and Ta_6 halide and oxyhalide series. Preliminary X-ray diffraction studies, performed both on powder and single crystals, indicated that $CsErTa_6Cl_{18}$ and $Cs_2UTa_6Cl_{15}O_3$ are isotypic with $CsLuNb_6Cl_{18}$[11] and $Cs_2LaTa_6Br_{15}O_3$,[8] respectively.

Crystal Structure Determination. Single crystals of $0.11 \times 0.11 \times 0.11$ mm^3 for $CsErTa_6Cl_{18}$ and $0.07 \times 0.10 \times 0.10$ mm^3 for $Cs_2UTa_6Cl_{15}O_3$ were selected for the structural determination. X-ray intensity data were collected at room temperature on an Enraf-Nonius CAD-4 four-circle diffractometer using graphite-monochromatized Mo Kα radiation. The unit-cell constants of the two compounds were determined from least-squares refinement of 25 reflections. Details of the data collection and refinement for $CsErTa_6Cl_{18}$ and $Cs_2UTa_6Cl_{15}O_3$ are given in Tables 1 and 2, respectively.

Intensity data treatment and refinement calculations were performed using the MOLEN program[12] on a digital Microvax 3100. The atomic scattering factors were taken from ref 13. The structures of the two compounds were solved by isotypy with final $R = 0.034$ and $R_w = 0.048$ for $CsErTa_6Cl_{18}$ and $R = 0.032$ and $R_w = 0.034$ for $Cs_2UTa_6Cl_{15}O_3$. At this stage of the study the final Fourier difference maps of the two compounds were featureless. The refinement of the site occupancies indicates that all the positions are fully occupied. Positional and thermal parameters are listed in Tables 3 and 4. Relevant interatomic distances and bond angles are given in Tables 5 and 6. Anisotropic thermal parameters and observed and calculated structure factors are available from the authors upon request.

Table 3. Positional and Isotropic-Equivalent Thermal Parameters for $CsErTa_6Cl_{18}$

atom	site	x	y	z	$B_{eq}{}^a$ (Å^2)
Ta	12i	0.19618(3)	0.03951(3)	0.56802(2)	0.550(5)
Cl1	12i	0.0839(2)	0.4489(2)	0.1613(1)	0.92(3)
Cl2	12i	0.4233(2)	0.1436(2)	0.0014(1)	0.86(3)
Cl3	12i	0.2353(2)	0.1891(2)	0.1619(1)	0.98(3)
Er	2d	$^2/_3$	$^1/_3$	$^3/_4$	0.80(1)
Cs	2c	$^2/_3$	$^1/_3$	$^1/_4$	5.84(8)

^{a} Equivalent isotropic B defined as $^4/_3\sum\sum a_i a_j B_{ij}$.

Table 4. Positional and Isotropic-Equivalent Thermal Parameters for $Cs_2UTa_6Cl_{15}O_3$

atom	site	x	y	z	$B_{eq}{}^a$ (Å^2)
Ta	12i	0.19215(3)	0.01372(3)	0.18268(2)	0.608(4)
C11	12i	0.6039(3)	0.5326(3)	0.1158(1)	1.51(4)
C13	12i	0.2048(2)	0.2202(2)	0.0863(1)	1.06(3)
C12	6h	0.2120(2)	0.424	$^1/_4$	1.03(4)
O	6h	0.1835(5)	0.367	$^3/_4$	0.9(1)
Cs	4f	$^2/_3$	$^1/_3$	0.54615(7)	1.96(1)
U	2c	$^2/_3$	$^1/_3$	$^1/_4$	0.854(9)

^{a} Equivalent isotropic B defined as $^4/_3\sum\sum a_i a_j B_{ij}$.

Table 5. Interatomic Distances (Å) and Bond Angles (deg) in $CsErTa_6Cl_{18}$

Ta−Ta	2.8758(6)	Ta−Cl3	2.452(2)
Ta−Ta	2.8727(6)	Ta−Cl3	2.464(2)
Cl2−Cl2	3.446(2)	Er−Cl1	2.657(2)
Cl3−Cl3	3.455(4)	Cs−Cl1	3.771(2)
Cl2−Cl3	3.403(3)	Cs−Cl3	3.828(2)
Cl2−Cl3	3.447(4)	Ta−Er	4.929(2)
Ta−Cl1	2.691(2)	Ta−Cs	5.260(2)
Ta−Cl2	2.466(2)	Cs−Er	5.334(2)
Ta−Cl2	2.471(2)		
Ta−Ta−Ta	59.96(1)	C13−Ta−C11	79.16(7)
Ta−Ta−Ta	60.07(2)	Cl2−Ta−Cl1	82.51(7)
Cl1−Er−Cl1	90.19(7)	Cl2−Ta−Cl1	80.63(7)
Cl3−Ta−Cl1	80.49(7)		

DFT Calculations. Density functional calculations[14] were carried out on different M_6X_{18} models using the Amsterdam density functional (ADF) program[15] developed by Baerends and co-workers.[16] This program is based on the Kohn−Sham approach to the density functional theory. This implies a one-electron picture of the many-electron systems but yields in principle exact electron density. The main

(10) Meyer, G.; Ax, P. *Mater. Res. Bull.* **1982**, *17*, 1447.
(11) Ihmaïne, S.; Perrin, C.; Sergent M. *Acta Crystallogr.* **1989**, *C45*, 705.
(12) Fair, C. K. *MOLEN: An Interactive Intelligent System for Crystal Structure Analysis*; Enraf-Nonius: Delft, The Netherlands, 1990.
(13) *International Tables for X-ray Crystallography;* The Kynoch Press: Birmingham, U.K., 1974; Vol. IV.
(14) For an introduction to density functional theory, see for example: (a) Parr, R. G.; Yang, W. *Density Functional Theory of Atoms and Molecules*; Oxford University Press: Oxford, 1989. (b) Ziegler, T. *Chem. Rev.* **1991**, *91*, 651. (c) Ziegler, T. *Can. J. Chem.* **1995**, *73*, 743. (d) Kohn, W.; Becke, A. D.; Parr, R. G. *J. Phys. Chem.* **1996**, *100*, 12974. (e) Baerends, E. J.; Gritsenko, O. V. *J. Phys. Chem.* **1997**, *A101*, 5384.
(15) *Amsterdam Density Functional (ADF) program*, Release 2.0.1; Vrije Universteit: Amsterdam, The Netherlands, 1996.
(16) (a) Baerends, E. J.; Ellis, D. E.; Ros, P. *Chem. Phys.* **1973**, *2*, 41. (b) Baerends, E. J.; Ros. P. *Int. J. Quantum. Chem.* **1978**, *S12*, 169. (c) Boerrigter, P. M.; te Velde, G.; Baerends, E. J. *Int. J. Quantum Chem.* **1988**, *33*, 87. (d) te Velde, G.; Baerends, E. J. *J. Comput. Phys.* **1992**, *99*, 84.

Table 6. Interatomic Distances (Å) and Bond Angles (deg) in $Cs_2UTa_6Cl_{15}O_3$

Ta−Ta	2.9529(6)	Cl2−Cl3	3.356(2)
Ta−Ta	2.9838(6)	Cl2−O	3.169(5)
Ta−Ta	2.7599(6)	Cl3−Cl3	3.386(4)
Ta−Cl1	2.578(2)	Cl3−Cl3	3.547(4)
Ta−Cl2	2.4575(7)	Cl3−O	3.273(3)
Ta−Cl3	2.474(2)	U−O	2.383(5)
Ta−Cl3	2.477(2)	U−C11	3.167(3)
Ta−O	1.959(2)	Cs−C11	3.489(2)
Ta−U	4.018	Cs−C11	3.528(3)
Ta−Cs	4.631	Cs−C12	3.993(1)
Cl1−Cl2	3.385(3)	Cs−C13	3.720(2)
Cl1−Cl3	3.352(3)	U−Cs	5.078
Cl1−Cl3	3.377(3)	Cs−Cs	5.533
Cl1−O	2.856(3)		
Ta−Ta−Ta	55.40(1)	Ta−Ta−Ta	87.68(1)
Ta−Ta−Ta	61.73(1)	Ta−Ta−Ta	92.01(1)
Ta−Ta−Ta	62.87(1)		

characteristics of the program are the use of a density fitting procedure to obtain Coulomb and exchange potentials in each SCF cycle, the numerical integration of the effective one-electron Hamiltonian matrix elements, and the possibility to free core orbitals. The numerical integration procedure requires one input parameter which determines the precision of numerical integrals.[15] The local-exchange correlation potential of Vosko−Wilk−Nusair was used for the local density approximation (LDA).[17] Relativistic (scalar relativistic (SR) formalism) corrections were incorporated for Nb and Ta.[18] The geometry optimization procedure was based on the method developed by Versluis and Ziegler.[19] A frozen-core approximation was used to treat the core electrons of Nb (1s4p), Ta (1s5p), Cl (1s2p), and Br (1s3p). The valence atomic orbitals were described by a double-ζ STO basis set for Cl 3s, 3p, and Br 3d, 4s, and 4p, a double-ζ STO basis set for Nb and Ta *n*d, $(n + 1)$s, augmented with a single-ζ $(n + 1)$p polarization function.

In some cases (see below), the electric field due to the countercations surrounding the $[M_6X^i_{12}X^a_6]^{n-}$ clusters was modeled by six point charges[15] of $n/6$ charge distributed around the cluster along the M−X^a directions 10 Å far away from the X^a ligands. Partial optimization was carried out by varying M−M distances and keeping fixed M−X^a and X^a−point charge distances.

Results and Discussion

Structural and Electronic Features of the Halide $A_xREM_6X_{18}$ Clusters. The structure of $CsErTa_6Cl_{18}$ is based on $(Ta_6Cl^i_{12}Cl^a_6)^{4-}$ units of D_{3d} symmetry, forming a ···AA′A··· pseudohexagonal stacking (see Figure 1a), with the units of the A′ layer rotated by about 22° with respect to the units of the A layer. The erbium and cesium cations are located at ($^2/_3$, $^1/_3$, $^3/_4$) and ($^2/_3$, $^1/_3$, $^1/_4$), respectively, lying in pseudo-trigonal prismatic environment of $(Ta_6Cl_{18})^{4-}$ units. Er^{3+} cations are bound to 6 bromine atoms which form a distorted octahedron of D_{3d} symmetry, whereas Cs^+ cations sit in the middle of a complex polyhedron made of 12 bromine atoms (see Figure 1a). The latter site is very large and asymmetrical, explaining the important and anisotropic thermal factor measured for the cesium atoms (see Table 3), as usually observed in all compounds exhibiting this structure type.

The $P\bar{3}1c$ structure of $CsErTa_6Cl_{18}$ illustrates the $CsREM_6X_{18}$ series which was obtained with all the combinations of RE = all the rare-earth metals, M = Nb or Ta, and X = Cl or Br. More recently, in the Ta/Cl system the rare-earth metal was replaced by a divalent alkaline-earth cation like Ba^{2+}, Pb^{2+}, Sr^{2+}, and Ca^{2+}.[20] In contrast, with monovalent cations smaller than Cs^+, such as K^+ or Rb^+ for instance, the M_6X_{18} units form a fcc staking ($R\bar{3}$ space group), although the A and RE cations remain 12X- and 6X-coordinated, respectively. The A site is most frequently statistically half-occupied corresponding to $x = 1$ in this case where RE is a trivalent rare-earth metal. On the other hand, this A site can be fully occupied ($x = 2$) when RE is a divalent rare-earth metal (Eu^{2+} and Yb^{2+}) or replaced by a divalent alkaline-earth cation. Finally, this site can be empty ($x = 0$) leading to the ternary REM_6X_{18} series, except for niobium bromides.[6]

The different solid-state compounds containing discrete M_6X_{18} units that we and others have characterized are reported in Table 7. Relevant average intra-unit interatomic distances are given. These compounds have generally a VEC of 14, 15, or 16. Amid the compounds we prepared, we noted that only 16-electron Nb_6 bromides were obtained, while both 15- and 16-electron Ta_6 bromine species could be synthesized. Nevertheless, crystals suitable for X-ray measurements were obtained only for the 16-electron Ta/Br compounds. On the other hand, crystals of both 15- and 16-electron Nb and Ta chlorine compounds could be grown. No compounds with 14 cluster valence electrons were isolated by solid-state chemistry routes.

The same relatively regular octahedral architectural unit is observed in all these structures, regardless of the electron count. There is, however, some significant lengthening of the M−M distances and some shortening of the M−X^a and M−X^i separations, respectively, with the diminution of the electron count (compare for instance the two isotypic compounds $KLuNb_6Cl_{18}$ and $LuNb_6Cl_{18}$).[25]

It is possible to construct the molecular orbital (MO) pattern of this type of cluster with the aid of symmetry and orbital overlap arguments.[4,5] For the sake of understanding, let us recall that it can qualitatively be derived from the interaction of the frontier orbitals (FO) of six square-pyramidal ML_5 fragments. Indeed, in the motif $(M_6X^i_{12})X^a_6$ of O_h symmetry, each transition metal is locally surrounded by four inner and one apical ligand which depict a square pyramid. Such ML_5 fragments present a radial hybrid (σ) situated above a "t_{2g}" set of d-type orbitals (two d(π) and one d(δ)).[34] In the O_h symmetry of the cluster, the six σ-hybrid FOs give rise to one bonding a_{1g}, three nonbonding (t_{1u}), and two antibonding (e_g) combinations. The d(π) FOs of the six entities generate sets of six bonding (t_{2g} and t_{1u}) and six antibonding combinations (t_{1g} and t_{2u}). Finally, the six d(δ) FOs give rise to one bonding (a_{2u}), three nonbonding

(17) Vosko, S. H.; Wilk, L.; Nusair, M. *Can. J. Phys.* **1980**, *58*, 1200.
(18) (a) Snjiders, J. G.; Baerends, E. J. *Mol. Phys.* **1978**, *36*, 1789. (b) Snjiders, J. G.; Baerends, E. J.; Ros, P. *Mol. Phys.* **1979**, *38*, 1909.
(19) Verluis, L.; Ziegler, T. *J. Chem. Phys.* **1988**, *88*, 322.
(20) Loisel, C.; Perrin, C. Unpublished results.
(21) Koknat, F. W.; McCarley, R. E. *Inorg. Chem.* **1972**, *11*, 812.
(22) Spreckelmeyer, B.; von Schnering, H. G. *Z. Anorg. Allg. Chem.* **1971**, *386*, 27.
(23) Thaxton, C. B.; Jacobson, R. A. *Inorg. Chem.* **1971**, *10*, 1461.
(24) Koknat, F. W.; McCarley, R. E. *Inorg. Chem.* **1974**, *13*, 295.
(25) Ihmaïne, S.; Perrin, C.; Peña, O.; Sergent, M. *J. Less-Common Met.* **1988**, *137*, 323.
(26) Simon, A.; von Schnering, H. G.; Schäfer, H. *Z. Anorg. Allg. Chem.* **1968**, *361*, 235.
(27) Lachgar, A.; Meyer, H.-J. *J. Solid State Chem.* **1994**, *110*, 15.
(28) Sitar, J.; Lachgar, A.; Womelsdorf, H.; Meyer, H.-J. *J. Solid State Chem.* **1996**, *122*, 428.
(29) Ihmaïne, S.; Perrin, C.; Sergent, M. *Acta Crystallogr.* **1987**, *C43*, 813.
(30) Bajan, B.; Meyer, H.-J. *Z. Naturforsch.* **1995**, *50b*, 1373.
(31) Ueno, F.; Simon, A. *Acta Crystallogr.* **1985**, *C41*, 308.
(32) Cordier, S.; Perrin, C.; Sergent, M. *Z. Anorg. Allg. Chem.* **1993**, *619*, 621.
(33) Cordier, S.; Perrin, C.; Sergent, M. *J. Solid State Chem.* **1995**, *118*, 274.
(34) (a) Johnston, R. L.; Mingos, D. M. P. *Inorg. Chem.* **1986**, *25*, 1661. (b) Mingos, D. M. P.; Lin, Z. *Z. Phys. D Atoms, Molecules and Clusters* **1989**, *12*, 53.

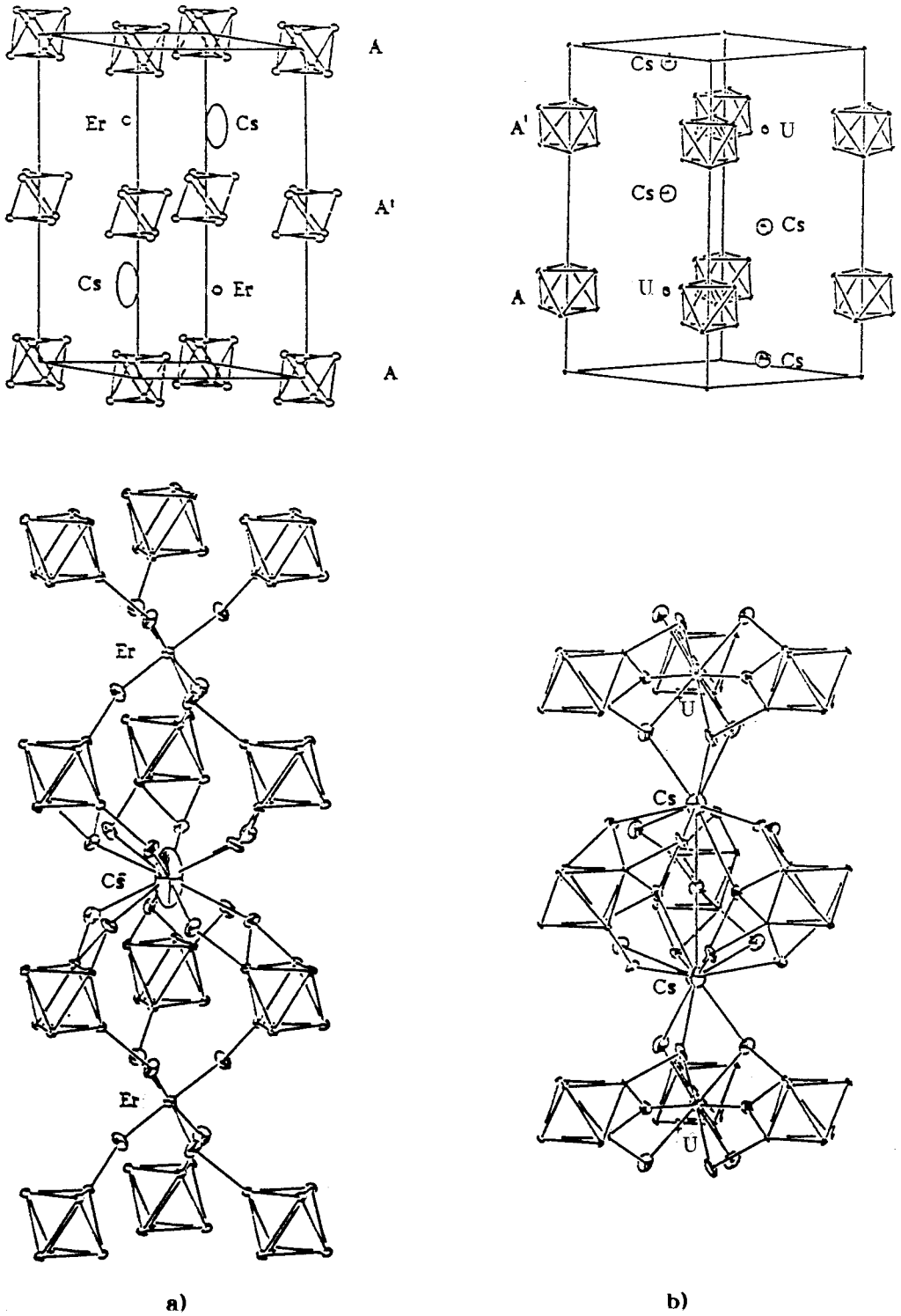

Figure 1. Unit cell (top, Cl and O atoms are not shown for clarity) and cation environment (bottom, only the Cl and O atoms involved in the cation coordination spheres are shown) in $CsErTa_6Cl_{18}$ (a) and $Cs_2UTa_6Cl_{15}O_3$ (b).

(t_{2g}), and two antibonding (e_u) combinations. Interaction between combinations of the same symmetry results in additional stabilization of the bonding t_{1u} and t_{2g} levels, whereas the nonbonding t_{1u} and t_{2g} combinations are destabilized and become antibonding. Therefore, a set of eight metal−metal bonding MOs and sixteen metal−metal antibonding MOs are expected for this kind of $(M_6X^i_{12})X^a_6$ unit. The complete occupation of the M−M bonding MOs fulfills the closed-shell requirement with an electron count of 16.

This qualitative analysis has been confirmed by all the MO calculations reported so far.[5,36] These calculations, which are all of the extended Hückel (EH) type, indicate that the M−M bonding δ-type a_{2u} combination, which is M−X^i antibonding, is the HOMO of the 16-electron species. However, the computed HOMO(a_{2u})-LUMO(e_u) gap (noted ΔE_2 in the followings) is always reported to be small, at variance with the experimentally observed stability and diamagnetism of the $(M_6X^i_{12})X^a_6$ compounds. Based on these results, clusters with

(35) Emsley, J. *The Elements*; Clarendon Press: Oxford, 1989.
(36) See for instance: (a) Pyykkö, P. *Chem. Rev.* **1988**, *88*, 563. (b) Kaltsoyannis, N. *J. Chem. Soc., Dalton Trans.* **1997**, 1 and references therein.

Table 7. Averaged Distances of the Structurally Characterized Compounds Containing Discrete M_6X_{18} (M = Nb, Ta; X = Cl, Br) Units[a]

compound	space group	VEC	M−M	M−X^i	M−X^a	ref
$(Me_4N)_2Nb_6Cl_{18}$	$P\bar{3}m1$	14	3.02	2.42	2.46	21
$(PyH)_2Nb_6Cl_{18}$	$R\bar{3}m$	14	3.04	2.43	2.48	22
$(PyH)_2Nb_6Br^i_{12}Cl^a_6$	$R\bar{3}m$	14	3.07	2.561	2.464	22
$(PyH)_2Nb_6Br^i_6Cl^i_6Br^a_6$	$R\bar{3}m$	14	3.03		2.616	22
$H_2(Ta_6Cl_{18})$, 6 H_2O	$Fd\bar{3}m$	14	2.962	2.414	2.507	23
$(Me_4N)_3Nb_6Cl_{18}$	$R\bar{3}$	15	2.967	2.430	2.520	24
$LuNb_6Cl_{18}$	$R\bar{3}$	15	2.956	2.431	2.623	25
$CsPbTa_6Cl_{18}$	$P\bar{3}1c$	15	2.925	2.439	2.574	20
$K_4Nb_6Cl_{18}$	C_2/m	16	2.910	2.480	2.596	26
$In_2Li_2Nb_6Cl_{18}$	$P\bar{1}$	16	2.929	2.457	2.613	27
$K_2MnNb_6Cl_{18}$	$R\bar{3}$	16	2.932	2.454	2.615	28
$KLuNb_6Cl_{18}$	$R\bar{3}$	16	2.916	2.452	2.654	25
$KGdNb_6Cl_{18}$	$R\bar{3}$	16	2.917	2.455	2.648	29
$CsLuNb_6Cl_{18}$	$P\bar{3}1c$	16	2.913	2.445	2.667	11
$In_4Ta_6Cl_{18}$	C_2/m	16	2.889	2.466	2.591	30
$Cs_2PbTa_6Cl_{18}$	$R\bar{3}$	16	2.888	2.462	2.595	20
$CsErTa_6Cl_{18}$	$P\bar{3}1c$	16	2.874	2.463	2.691	this work
$K_4Nb_6Br_{18}$	C_2/m	16	2.971	2.592	2.793	31
$Cs_2EuNb_6Br_{18}$	$R\bar{3}$	16	2.970	2.595	2.804	32
$CsErNb_6Br_{18}$	$P\bar{3}1c$	16	2.954	2.587	2.885	32
$CsErTa_6Br_{18}$	$P\bar{3}1c$	16	2.898	2.587	2.892	33

[a] The compounds with the same space group are isotypic.

14 rather 15 or 16 electrons should be favored. This suggests that EHMO calculations somewhat fail to reproduce correctly the balance between M−M and M−X interactions in these clusters. This is one of the reasons why we have carried out DFT calculations in order to study in a more quantitative way the relationship between the nature of the metal atoms and the ligands and the electron count in this type of cluster. Different halide $[(M_6X^i_{12})X^a_6]^{n-}$ structures were computed. The main results are given in Table 8.

A comparison of the M−M separations measured in the crystal structures of different $[(M_6X^i_{12})X^a_6]^{n-}$ (n = 2, 3, 4) cluster compounds indicates that with the same ligand environment, Ta−Ta and Nb−Nb distances are comparable (Ta−Ta distances are actually slightly shorter than the corresponding Nb−Nb ones, see Table 7). It is known that third-row transition-metal elements are of similar size to their second-row counterparts. For instance, niobium and tantalum both have a metallic radius of 1.43 Å.[35] This size contraction effect observed for third-row atoms relies on a complicated interplay of shell-structure and relativistic effects.[36,37]

As expected, a marked reduction in the bond lengths involving tantalum atoms is found for the $[(Ta_6X^i_{12})X^a_6]^{n-}$ species on moving from nonrelativistic (NR) to relativistic (SR) calculations. Geometry optimizations performed on different $[(Ta_6Cl^i_{12})Cl^a_6]^{n-}$ and $[(Ta_6Br^i_{12})Br^a_6]^{n-}$ (n = 2, 3, 4) models show that relativistic corrections are necessary for a correct description of these systems. A contraction of the Ta−Ta bond lengths of ca. 5% is computed when relativistic effects are taken into account in the calculations. They are not so essential for the Nb systems. A Nb−Nb contraction of ca. 1% is observed when relativistic effects are taken into account.

The computed Nb−Nb and Ta−Ta separations are in the range of 2.97−3.08 and 2.91−3.00 Å, respectively. They compare rather well with the bond lengths measured in the available X-ray structures (see Tables 7 and 8), giving confidence in the computed bond distances for complexes which are not yet synthesized. For the 14-electron species, the maximum M−M bond length difference between computed and experimental distances is lower than 0.02 Å. A somewhat larger deviation is noticed as the VEC increases. For instance the computed Ta−Ta separations in the 16-electron $[(Ta_6Br^i_{12})Br^a_6]^{4-}$ model are 0.07 Å longer than the Ta−Ta distances measured in $CsErTa_6Br_{18}$ (2.96 vs 2.89 Å).

A contraction of the M−M bonds is observed upon the augmentation of the VEC both in niobium and tantalum chlorides models. This trend, which is observed experimentally, is related to the weakly metal−metal bonding character of the a_{2u} MO (see above).

A rather good agreement is also observed between the computed and experimental values of the M−X^i and M−X^a distances (see Tables 7 and 8). Nevertheless, as in the case of the M−M distances, the M−X^a separations are computed somewhat too long when the VEC increases. This is probably because the electrostatic interactions caused by the countercation are not included in the calculations. A shortening is noted for the M−M and M−X^a separations (ca. 0.2−0.4 Å) when point charges, used to modelize the electric field created by the cations around the cluster in the solid, are included in the calculations on $[(M_6X^i_{12})X^a_6]^{4-}$ models (see computational details in the Experimental Section). Indeed, the experimental M−X^a distances and to a lesser extent the M−M separations are quite sensitive to the nature of the cationic sphere surrounding the $(M_6X^i_{12})X^a_6$ units. For instance, Nb−Br^a bond lengths are 2.88 Å in $CsErNb_6Br_{18}$ and 2.80 Å in $Cs_2EuNb_6Br_{18}$ (see Table 7).

Contrarily to the previous EHMO studies which found ΔE_2 too small (see above),[5,34] the DFT calculations find the a_{2u} level lying in the middle of a large energy gap between the bonding t_{2g} and the antibonding e_u levels ($\Delta E_1 \approx \Delta E_2$) (see Figure 2 and Table 8). This new important result is in full agreement with the existence of two favored closed-shell electron counts of 14 and 16, as well as with the intermediate one of 15. The fact that ΔE_1 is even smaller than ΔE_2 is consistent with the largest occurrence in the solid state of 16-electron $[(M_6X^i_{12})X^a_6]^{n-}$ species, compared to their 14- and 15-electron homologues.

According to DFT MO diagrams shown in Figure 2 for different 14-VEC models, the energy gap ΔE_1 hardly varies regardless of the nature of the metal. On the other hand, it somewhat varies upon the nature of the ligands. It decreases from ca. 0.5 eV for the chlorides to ca. 0.4 eV for the bromides. The M−M bonding and M−X^i antibonding a_{2u} MO is ca. 60% metal and 40% X^i ligand in character. For symmetry reasons, it does not possess any X^a participation. In addition to a strong metal character, the lower M−M bonding occupied cluster MOs, a_{1g}, t_{1u}, and t_{2g}, have also an important X^a contribution. They are M−M bonding and slightly M−X^a antibonding. Consequently, the width of the energy gap ΔE_1 is mainly controlled by the nature of the apical X^a ligand. Increasing of the M−X^a antibonding character leads to the destabilization of these MOs. This is expected to occur when the electronegativity of the apical ligands gets closer to that of the metal. This is the case for bromine compared to chlorine. The bromine AOs, higher in energy than the chlorine AOs, enhance the destabilization of the metallic FMOs they interact with, diminishing ΔE_1.

Contrarily to ΔE_1, the energy gap ΔE_2 strongly varies upon the nature of the metal. Indeed, it increases from ca. 0.70 eV with Nb to over 1.4 eV with Ta, regardless of the surrounding ligands. The lowest vacant MOs positioned above the a_{2u} MO are strongly metallic in character (>80%), with a small X^i contribution. The magnitude of their M−M antibonding

(37) (a) Ziegler, T.; Snijders, G. J.; Baerends, E. J. *Chem. Phys. Lett.* **1980**, *75*, 1. (b) Snijders, G. J.; Pyykkö, P. *Chem. Phys. Lett.* **1980**, *75*, 5. (c) Ziegler, T.; Snijders, G. J.; Baerends, E. J. *J. Chem. Phys.* **1981**, *74*, 1271.

Table 8. Optimized Geometries and Corresponding ΔE_1 and ΔE_2 Energy Gaps[a] for Selected $[M_6X^i_{12}X^a_6]^{n-}$ (M = Nb, Ta; X = Cl, Br) Models

n charge	2	3	4
	M−M Bond Distances (Å)		
Nb_6Cl_{18}	3.018 (3.020−3.040)[b]	3.003 (2.956−2.967)	2.967 (2.910−2.932)
Nb_6Br_{18}	3.081	3.041	3.020 (2.954−2.971)
Ta_6Cl_{18}	2.972 (2.962)	2.945 (2.925)	2.911
Ta_6Br_{18}	3.004	2.993	2.965 (2.898)
	M−X^i Bond Distances (Å)		
Nb_6Cl_{18}	2.449 (2.42−2.43)	2.486 (2.430−2.431)	2.512 (2.445−2.480)
Nb_6Br_{18}	2.560	2.590	2.627 (2.587−2.595)
Ta_6Cl_{18}	2.549 (2.414)	2.566 (2.439)	2.587
Ta_6Br_{18}	2.627	2.668	2.680 (2.587)
	M−X^a Bond Distances (Å)		
Nb_6Cl_{18}	2.472 (2.46−2.48)	2.538 (2.520−2.623)	2.662 (2.596−2.667)
Nb_6Br_{18}	2.663	2.745	2.830 (2.793−2.885)
Ta_6Cl_{18}	2.551 (2.507)	2.597 (2.574)	2.644
Ta_6Br_{18}	2.738	2.795	2.852 (2.892)
	ΔE_1 and ΔE_2 Energy Gaps[a] (eV)		
Nb_6Cl_{18}	0.507/0.701	0.582/0.905	0.640/1.106
Nb_6Br_{18}	0.381/0.811	0.466/0.990	0.531/1.115
Ta_6Cl_{18}	0.591/1.443	0.650/1.591	0.738/1.756
Ta_6Br_{18}	0.428/1.333	0.456/1.664	0.680/1.671

[a] See text and Figure 2. [b] Experimental distances in brackets (see Table 7).

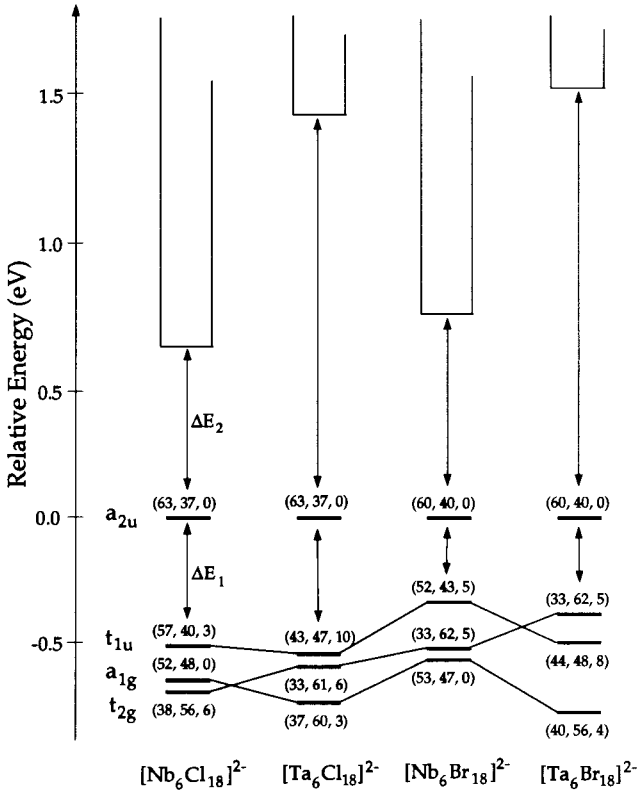

Figure 2. SR-DFT energy level diagrams for 14-electron $[M_6X^i_{12}X^a_6]^{2-}$ (M = Nb, Ta; X = Cl, Br) models. Numbers in brackets indicate the percentage of M, X^i, and X^a, respectively.

character governs the width of ΔE_2. Ta−Ta interactions are stronger than Nb−Nb interactions. This reflects in the total width of the metallic d band, larger for tantalum than for niobium (ca. 2.0 vs 2.8 eV). Consequently, the energy gap between the M−M bonding and antibonding sets is larger for Ta than for Nb.

To gain more confidence in our conclusions, mixed $(M_6X^i_{12})$-X'^a_6 models were computed. For instance, calculations on $(Nb_6Cl^i_{12})Br^a_6$ give an energy gap ΔE_1 of 0.44 eV, comparable to that observed for the all-bromine species, and an energy gap ΔE_2 of 0.65 eV, similar to that computed for Nb−Cl and Nb−Br models.

The same trend is observed for 15- and 16-VEC models. We just note a slight increase of both ΔE_1 and ΔE_2 upon augmentation of the cluster electron count. This is due to the contraction of the octahedral core upon electron addition, which increases the dispersion of the metallic band.

In summary, contrarily to what we may expect at first sight, energy gaps ΔE_1 and ΔE_2 do not depend on the energy of the a_{2u} MO. Its energy and nature are constant overall, regardless of the nature of the metal and ligands. ΔE_2 is rather imposed by the nature of the metal, whereas ΔE_1 is mainly governed by the nature of the surrounding apical ligands. The particularly small ΔE_1 gaps computed for the bromine clusters (see Table 8) lead us to propose that $(M_6Br^i_{12})Br^a_6$ species should be observed with 16 electrons more easily than $(M_6Cl^i_{12})Cl^a_6$ compounds.

As said earlier, the a_{2u} level is M−M bonding and M−X^i antibonding. We may expect therefore some shortening of the M−M separations and some lengthening of the M−X^i separations upon electron addition. This is in agreement with the experimental and optimized geometries given in Table 8. Nevertheless, despite the fact that this MO does not have any X^a contribution, we observe also some M−X^a lengthening. DFT Walsh diagrams corresponding to the approach of the six apical ligands around the $M_6X^i_{12}$ fragment show that the potential energy of the clusters increases very sharply for X^a−X^i separations of ca. 3.2 and 3.4 Å for Cl and Br, respectively. This energy wall reflects some X^a−X^i steric hindrance, which is alleviated by M−X^a bond lengthening. Therefore, the fact that the M−X^a distances lengthen quite sharply upon electron addition, indicates that the M−X bond lengthening in these kind of cluster is not only due to throughbond electronic factors but also to throughspace steric and electrostatic factors. Let us note that examination of the Walsh diagrams corroborates the fact that ΔE_1 depends strongly on X^a ligands. ΔE_1 decreases as the X^a ligands approach the $M_6X^i_{12}$ fragment.

Table 9 shows the atomic net charges for several $(M_6X^i_{12})$-X^a_6 clusters obtained using the Hirshfeld analysis.[38,39] The metal

(38) Hirshfeld, F. L. *Theor. Chim. Acta* **1977**, *44*, 129.

Table 9. Computed Hirshfeld Charges in Selected $[M_6X^i_{12}X^a_6]^{n-}$ (M = Nb, Ta; X = Cl, Br) Models

n charge	2	3	4
	M		
Nb_6Cl_{18}	0.17	0.16	0.14
Nb_6Br_{18}	0.14	0.13	0.11
Ta_6Cl_{18}	0.10	0.08	0.06
Ta_6Br_{18}	0.06	0.04	0.04
	X^i		
Nb_6Cl_{18}	−0.07	−0.12	−0.16
Nb_6Br_{18}	−0.05	−0.10	−0.13
Ta_6Cl_{18}	−0.03	−0.07	−0.12
Ta_6Br_{18}	−0.01	−0.04	−0.09
	X^a		
Nb_6Cl_{18}	−0.35	−0.41	−0.48
Nb_6Br_{18}	−0.37	−0.43	−0.50
Ta_6Cl_{18}	−0.36	−0.40	−0.48
Ta_6Br_{18}	−0.39	−0.44	−0.50

atoms are slightly positive and the inner X^i ligands are sligthly negative. Regardless of the cluster electron count, they remain roughly constant. In contrast, the outer X^a ligands are largely negative, being less involved in M−X bonding than the inner X^i ligands. Their negative charge increases upon the increase of the VEC. This indicates that the M−X^i bonds are essentially covalent in nature, whereas the M−X^a bond are rather ionic in character. We note that the Nb−X^a bonds are sligthly more polarized than the Ta−X^a bonds.

To analyze the metal−ligand and ligand−ligand interaction energies, the extended transition state (ETS) energy decomposition scheme proposed by Ziegler et al. may be used. According to this method,[40,41] the total bond energy, E_{tot}, between two fragments can be decomposed into a number of terms. Among these terms, one is appropriately called the steric repulsion energy, E_{steric}. It is made up of two components. One corresponds to the attractive electrostatic interactions (ionicity), and the other accounts for the repulsive two-orbital four-electron interactions between occupied orbitals on both fragments.[40] The other important term represents the stabilizing electronic interaction energy, E_{orb}, due to orbital interactions between vacant and occupied fragment orbitals. E_{orb} corresponds to the covalent bonding interactions. The homolytic approach (M· + X·) was chosen for the analysis.

The comparison of the total bond energy E_{tot} indicates that regardless of the VEC and the metal into play, the bonding is stronger for X = Cl than for X = Br (see Table 10). This is mainly due to the fact that E_{orb} is larger in absolute value for M−Cl bonds than for M−Br bonds. In other words, the M−Cl bonds are more covalent than M−Br bonds. To a lesser extent, this is also due to the fact that the steric repulsion energy between M and Cl is smaller than that between M and Br. Due to a more important orbital interaction energy between M and X (see Table 10), tantalum clusters are more likely to exist than the niobium analogues. In résumé, for a given electron count

Table 10. Decomposition of the Bonding Energy for Selected $[M_6X^i_{12}X^a_6]^{n-}$ (M = Nb, Ta; X = Cl, Br) Models

n charge	2	3	4
	E_{ste}[a] (eV)		
Nb_6Cl_{18}	95.77	99.80	93.18
Nb_6Br_{18}	101.41	94.05	85.52
Ta_6Cl_{18}	131.20	126.52	122.16
Ta_6Br_{18}	128.26	123.52	113.73
	E_{orb}[a] (eV)		
Nb_6Cl_{18}	−203.66	−207.04	−197.00
Nb_6Br_{18}	−201.88	−194.22	−182.38
Ta_6Cl_{18}	−246.74	−241.49	−233.50
Ta_6Br_{18}	−236.26	−231.17	−217.99
	E_{tot}[a] (eV)		
Nb_6Cl_{18}	−107.84	−107.23	−103.82
Nb_6Br_{18}	−100.47	−100.16	−96.85
Ta_6Cl_{18}	−115.53	−117.97	−111.32
Ta_6Br_{18}	−108.23	−107.67	−104.25

[a] E_{ste}, E_{orb}, and E_{tot} are computed from the formal reaction: 6M + 18X + ne^- → $[M_6X_{18}]^{n-}$.

Table 11. Averaged Distances of the Structurally Characterized M_6X_{18} (M = Nb, Ta; X = O, Cl, Br) Oxyhalides

compound	space group	VEC	M−M	M−X^a	ref
$Cs_2LuNb_6Cl_{17}O$	$R\bar{3}$	16	2.916	2.692	9
$Cs_2UNb_6Cl_{15}O_3$	$P\bar{3}1c$	14	2.948	2.581	42
$Cs_2UTa_6Cl_{15}O_3$	$P\bar{3}1c$	14	2.912	2.578	this work
$Cs_2LaTa_6Br_{15}O_3$	$P\bar{3}1c$	14	2.945	2.738	8
$ScNb_6Cl_{13}O_3$	$I4_122$	14	2.943	2.595	7
$LuTa_6Br_{13}O_3$	$I4_122$	14	2.939	2.762	43
$Ti_2Nb_6Cl_{14}O_4$	C_2/c	14	2.927	2.607	44

the bonding energy of the $(M_6X^i_{12})X^a_6$ clusters is mainly controlled by M−X^i interactions. The closer the electronegativity between M and X, the stronger the bonds in $(M_6X^i_{12})X^a_6$ cluster.

Structural and Electronic Features of the $A_xREM_6X_{18-y}O_y$ (x = 0, 2, y = 1, 3) Oxyhalides. No magnetic interaction between paramagnetic 15-electron clusters and magnetic cations has been observed so far in $A_xREM_6X_{18}$ compounds. This may be due to rather long separations between clusters and rare earth cations. One way to shorten such separations is for instance to diminish the size of the clusters by replacing large halogen ligands by small oxygen ligands. Attempts to synthesize new oxyhalide $A_xREM_6X_{18-x}O_x$ compounds containing magnetic and nonmagnetic rare earth cations were successful. Indeed, we were able to isolate for the first time three series of M_6 oxyhalides: $M_2RENb_6Cl_{17}O$,[9] $M_2REM_6X_{15}O_3$,[8,42] and $REM_6X_{13}O_3$.[7,43] The crystal structures of some of them were determined (see Table 11). Very recently, a species with four oxygen atoms, namely, $Ti_2Nb_6Cl_{14}O_4$, was characterized.[44]

The 16-electron $[(Nb_6Cl^i_{11}O^i)Cl^a_6]^{5-}$ units are contained in $A_2REM_6X_{17}O$.[9] The oxygen atom statistically occupies the inner positions around the octahedral clusters. Despite the presence of this oxygen atom, M−M bond lengths are nearly similar and M−X^i distances are longer overall than those in the parent cluster $[(Nb_6Cl^i_{12})Cl^a_6]^{4-}$ encountered in $KLuNb_6Cl_{18}$.[24] This may come from a charge effect which is more important in the oxyhalide compound.

The structure of $Cs_2UTa_6Cl_{15}O_3$ contains $[Ta_6(Cl^i_9O^i_3)Cl^a_6]^{5-}$ units of D_3 symmetry (see **2** in Chart 2) (apical Cl^a ligands are

(39) In contrast to the Mulliken population analysis, the Hirshfeld method yields atomic charges which are essentially stable against basis sets variations and correctly reflect the electronegativity differences between the atoms. See for instance: Bickelhaupt, F. M.; van Eikama Hommes, N. J. R.; Guerra, C. F.; Baerends, E. J. *Organometallics* **1996**, *15*, 2923.

(40) (a) Ziegler, T.; Rauk, A.; Bearends, E. J. *Theor. Chem. Acta* **1977**, *43*, 261. (b) Ziegler, T.; Rauk, A. *Theor. Chem. Acta* **1977**, *46*, 1. The method is an extension of the well-known decomposition scheme proposed by Morokuma (*J. Chem. Phys.* **1971**, *55*, 1236).

(41) For recent applications of the method see for instance: (a) Jacobsen, H.; Ziegler, T. *Inorg. Chem.* **1996**, *35*, 775. (b) Li, J.; Dickson, R. M.; Ziegler, T. *J. Am. Chem. Soc.* **1995**, *117*, 11482. (c) Rosa, A.; Baerends, E. J. *Inorg. Chem.* **1994**, *33*, 584.

(42) Cordier, S.; Perrin, C.; Sergent, M. *Mater. Res. Bull.* **1997**, *32*, 85.

(43) Cordier, S.; Perrin, C.; Sergent, M. *Croat. Chem. Acta* **1995**, *68*, 781.

(44) Anokhina, E. V.; Essig, M. V.; Lachgar, A. *Angew. Chem., Int. Ed.* **1998**, *37*, 522.

Table 12. Averaged Optimized Geometries and Corresponding ΔE_1 and ΔE_2 Energy Gaps[a] for Selected $[Nb_6Cl_{17}O]^{n-}$ ($n = 3, 4, 5$) and $[Nb_6Cl_{15}O_3]^{5-}$ Models

				$[Nb_6Cl_{13}O_3]^{5-}$	
compound	$[Nb_6Cl_{17}O]^{3-}$	$[Nb_6Cl_{17}O]^{4-}$	$[Nb_6Cl_{17}O]^{5-}$	C_2 isomer	D_3 isomer
			Bond Distances (Å)		
M−M[b]	3.039	3.015	3.007 (2.916)[c]	3.039 (2.943)	3.042 (2.948)
M−Cl^i	2.485	2.522	2.566	2.582 (2.452)	2.584 (2.470)
M−O^i	1.901	1.932	1.951	1.943 (1.991)	1.941 (1.956)
M−X^i *b*	2.460	2.497	2.540 (2.465)		
M-Cl[a]	2.545	2.637	2.732 (2.692)	2.741 (2.595)	2.722 (2.581)
			ΔE_1 and ΔE_2 Energy Gaps[a] (eV)		
ΔE_1	0.472	0.620	0.754	0.607	1.456
ΔE_2	0.575	0.729	0.826	0.177	0

[a] See text and Figure 2. [b] Averaged. [c] Experimental distances in brackets (see Table 11).

Chart 2

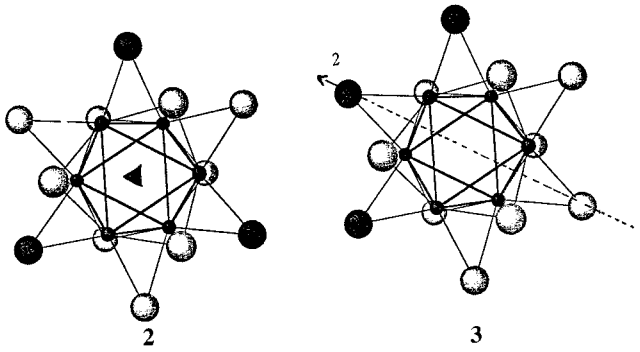

not shown for clarity) centered on the *c* axis located at $z = {}^1/_4$ and ${}^3/_4$ (see Figure 1b). The cluster units are strongly distorted due to the size effect of the oxygen compared to that of chlorine. It is strongly related to the $CsErTa_6Br_{15}O_3$ structure described above and to the $Cs_2LaTa_6Br_{15}O_3$ structure reported previously.[8] The units centered at (0, 0, 0) and (0, 0, ${}^1/_2$) in the halide compound are shifted of 1/4 along the *c* axis in the oxychloride species, leading to new cationic polyhedral sites. Indeed, two cesium cations per formula are present in this compound instead of one in the halide one. The uranium atom is surrounded by six Cl^a and three O^i belonging to three adjacent units, whereas the cesium atoms are bound to six Cl^i and six Cl^a belonging to six adjacent units (see Figure 1b). The latter site is smaller and more isotropic than in the halide structure as confirmed by the thermal factor values. The U−Cl^a distances are consistent with trivalent uranium cations as in $Cs_2UNb_6Cl_{15}O_3$,[42] leading to a VEC of 14 for the $(Ta_6Cl_{15}O_3)$.$^{5-}$

An alternative arrangement of C_2 symmetry with three adjacent oxygen atoms is observed for the 14-electron $[(M_6X^i{}_9O^i{}_3)X^a{}_2X^{a-a}{}_{4/2}]^{3-}$ units present in $REM_6X_{13}O_3$ (see **3** Chart 2).[7] One of the oxygen atoms is located along the 2-fold axis. No 15-electron species were characterized so far in this octahedral cluster oxyhalide chemistry.

Diffferent characteristics obtained from DFT calculations for the 16-electron $[(Nb_6Cl^i{}_{11}O^i)Cl^a{}_6]^{5-}$ and 14-electron $[(Nb_6Cl^i{}_9O^i{}_3)Cl^a{}_6]^{5-}$ models are given in Table 12. The results concerning $[(Nb_6Cl^i{}_{11}O^i)Cl^a{}_6]^{5-}$ are comparable to those given earlier for $(Nb_6Cl^i{}_{12})Cl^a{}_6$ clusters (see Table 8). In particular, ΔE_1 and ΔE_2 energy gaps are of the same order (see Tables 8 and 12). The same trends, i.e., increasing of the M−M bond lengths is computed upon the decrease of the VEC. As noticed earlier for the M_6X_{18} models, the computed optimized separations are slightly longer than the experimental ones since the charge effects of the countercations were not taken into account in the calculations. The presence of only one oxygen ligand does not modify too much the electronic and structural properties of these octahedral species.[45]

The comparison between the computed and experimental geometries for the 14-electron D_3 and C_2 $[(Nb_6Cl^i{}_9O^i{}_3)Cl^a{}_6]^{5-}$ isomers is also quite satisfactory (see Table 12). Here again, the charge effect of the surrounded cations being not taken into account, the computed metal cages are slightly larger than the experimental ones. As experimentally observed, the Nb−Cl^i distances adjacent to M−O^i bonds are longer than the nonadjacent ones (2.643 vs 2.556 Å and 2.650 vs 2.548 Å in D_3 and C_2 isomers, respectively).[7,8,42,43] Their electronic structure differs slightly from that of $[(Nb_6Cl^i{}_9O^i{}_3)Cl^a{}_6]^{5-}$ and M_6X_{18} models. The ΔE_1 energy gap remains substantial and comparable to those computed for the other models. On the other hand, the ΔE_2 energy gap becomes smaller in the C_2 isomer and disappears in the D_3 isomer (see Table 12) with the "a_{2u}" MO (a_2 in D_3 symmetry) lying among the M−M antibonding band. The destabilization of this MO is mainly due to the M−O^i antibonding character, more important in the D_3 isomer than in the C_2 isomer. The SR-DFT calculations indicate that the former isomer is more stable than the latter isomer by 0.44 eV. This results are in agreement with the experimental data. All structurally characterized $Cs_2REM_6X_{15}O_3$ compounds contain isolated units of D_3 symmetry.

Species containing 15-electron $[(M_6X^i{}_9O^i{}_3)X^a{}_6]^{6-}$ or 16-electron $[(M_6X^i{}_9O^i{}_3)X^a{}_6]^{7-}$ units seem unlikely because of the large ΔE_1 energy gap and also the important anionic charge which requires a large countercationic charge. This may prevent the synthesis of $A_xREM_6X_{18-x}O_x$ species with a large number of oxygen ligands. Attempts to synthesize such compounds with more than three oxygen ligands were unproductive so far. We did not obtain for instance $Cs_2U^{IV}Nb_6Cl_{14}O_4$ which would contain 14-electron $[(Nb_6Cl^i{}_8O^i{}_4)Cl^a{}_6]^{6-}$ units.[44]

Characterized 14-electron Nb_6 and Ta_6 halide clusters have rather long M−M and rather short M−X^a separations. It is worth mentioning that they cocrystallize with organic cations (see Table 7). Cocrystallizing with inorganic cations would increase ionic interactions between clusters and cations, leading to some lengthening of the M−X^a distances. As a consequence, this would somewhat destabilize the clusters. By allowing some shrinking of the octahedral metal core, inner oxygen atoms counterbalance this destabilizing effect, leading to the synthesis of 14-electron species cocrystallizing with inorganic cations. For instance, M−M and M−X^a distances measured for the 14-electron $(Nb_6Cl^i{}_9O^i{}_3)Cl^a{}_6$ units in $Cs_2UNb_6Cl_{15}O_3$ and $ScNb_6$-

(45) This is also true for fully oxygenated octahedral clusters. See for example: (a) Burdett, J. K.; Hughbanks, T. *J. Am. Chem. Soc.* **1984**, *106*, 3101. (b) Reference 3.

$Cl_{13}O_3$ are close to those observed for the 16-electron cluster $(Nb_6Cl^i_{12})Cl^a_6$ present in $KLuNb_6Cl_{18}$.

Conclusion

This investigation emphasized the reasons why edge-bridged octahedral cluster M_6X_{18} are widely observed for several electron counts, in particular for 16 electrons. In contrast to previous EH calculations, DFT results show a level of a_{2u} symmetry lying in the middle of a large energy gap separating a bonding set of MOs from an antibonding set of MOs. The energy and nature of this level are constant overall. The energy gap between this a_{2u} MO and the bonding ones depends on the energy of the latters, which is mainly governed by the nature of the apical X^a ligands. On the other hand, the gap separating the a_{2u} MO from the antibonding block depends on the nature of the metal into play. Tantalum octahedral clusters surrounded by chlorine ligands exhibit stronger bonding. Replacing one X ligand by a less-hindered oxygen ligand does not modify much the electronic structure of these species. Stable $M_6X_{17}O$ clusters with different electron counts are theoretically possible. Only one example with 16 electrons has been experimentally observed so far.[9] A larger number of oxygen ligands perturbs the electronic structure, and 14-electron species are likely to be trapped, as experimentally observed in the case of $M_6X_{15}O_3$ compounds.[7,8,42,43]

Acknowledgment. Prof. Baerends and Dr. te Velde (Vrije Universiteit, Amsterdam) are acknowledged for introducing the authors to the ADF program. Exchanges between the groups of Amsterdam and Rennes have been made possible through a European Human Capital and Mobility Network (ERBCHRXCT-930156). J.-F.H. and J.-Y.S. thank the Centre de Ressources Informatiques (CRI) of Rennes and the Institut de Développement et de Ressources en Informatique Scientifique (IDRIS-CNRS) of Orsay (Project 970649) for computing facilities.

Supporting Information Available: Tables listing thermal displacement parameters (4 pages). Ordering information is given on any current masthead page.

IC980328H